Tight-binding calculations of the band structure and total energies of the various polytypes of silicon carbide

N. Bernstein, H. J. Gotsis,* D. A. Papaconstantopoulos, and M. J. Mehl
Center for Computational Materials Science, Naval Research Laboratory, Washington, DC 20375, USA
(Received 24 November 2003; revised manuscript received 23 November 2004; published 16 February 2005)

We present electronic structure and total energy calculations for SiC in a variety of polytype structures using the NRL nonorthogonal tight-binding method. We develop one set of parameters optimized for a combination of electronic and energetic properties using a *sp* basis, and one optimized for electronic properties using a *spd* basis. We compute the energies of polytypes with up to 62 atoms per unit cell, and find that the hexagonal wurtzite structure is highest in energy, the 4H structure is lowest in energy, and the cubic zinc-blende structure is in between, in agreement with our linear augmented plane-wave and other calculations. For the *sp* model we find that the electronic structure of the cubic and hexagonal structures are in good agreement with density-functional theory calculations only for the occupied bands. The *spd* parametrization optimized for the electronic structure of the zinc-blende and wurtzite structures at the equilibrium volume reproduces nearly perfectly both the valence and conduction bands. The *sp* tight-binding model also yields elastic constants, phonon frequencies, stacking fault energies, and vacancy formation energies for the cubic structure in good agreement with available experimental and theoretical calculations. Using molecular dynamics simulations we compute the finite-temperature thermal expansion coefficient and atomic mean-square displacements in good agreement with available first-principles calculations.

DOI: 10.1103/PhysRevB.71.075203 PACS number(s): 71.15.Nc, 71.15.Pd, 71.20.Nr

I. INTRODUCTION

Silicon carbide is an interesting material in three important respects. From a theoretical point of view, it appears to be the prototype polytypic substance[1] with endless permutations of stacking sequences theoretically possible. The polytypes are characterized by a stacking sequence with a long repeat unit along the stacking axis and therefore are natural superlattices. It is also the most attractive alternative to silicon for high-temperature, high-power device applications because of several inherent material advantages.[2–5] These advantages are a large energy band gap, large thermal conductivity (close to that of copper), high hardness, and high saturation value of electron drift velocity. Finally, there is body of data[6] regarding electronic, optical, transport, and structural properties, against which theory and calculations can be assessed.

The polytypes of SiC differ in the stacking order of double layers of Si and C atoms. More than 200 polytypes have been reported to date. Luckily, only a few of them have practical importance. These include the cubic zinc-blende (zb) structure or 3C, and the 4H and 6H hexagonal forms, which appear to have the lowest energy. The 2H form (also known as wurtzite), although rare in SiC, is of interest as the extreme hexagonal case. One distinguishes three different layers, denoted by A, B, and C, corresponding to different positions of the atoms in planes perpendicular to the *c* axis, which is the stacking direction. In this notation, the simplest polytypes are the 3C with a stacking order ABC and the 2H with AB. One of the most stable polytypes, 6H SiC, contains six SiC pairs per unit cell and has stacking sequence ABCACB. Noting that an ACB block is nothing but an ABC block rotated by 60° about the stacking axis, the 6H structure can be regarded as an alternating sequence of unrotated and rotated ABC blocks. All other polytypes can be built up in a similar way. The basic physics of the polytypes' energetics can be modeled by an axial-next-nearest-neighbor Ising (ANNNI) model,[7,8] which associates a pseudospin with each stacking sequence (+1 for cubic, −1 for hexagonal). The ANNNI model is a good approximation, but it cannot give insight into the factors that determine the effective coupling parameters, and, as noted in Ref. 8, the mechanism by which short-range bare interactions combine to produce effective long-range ANNNI interactions is implausible, at least for SiC. Early first-principles computational work addressing the polytype stability question is reviewed in Refs. 9 and 10.

The ground state properties of cubic SiC have been calculated using density-functional theory (DFT) with the plane-wave pseudopotential method.[11,12] The calculated properties, such as equilibrium lattice constant, bulk modulus, and its pressure derivative, agree with the available experimental data to within a few percent. Similar calculations have been done for the 2H form of SiC,[13] and the calculated lattice parameters and bulk modulus are also in agreement with experiment. The structural and electronic properties of cubic, 2H, 4H, and 6H SiC have been calculated by the *ab initio* pseudopotential method.[14] The lattice constants, bulk moduli, and their pressure derivatives are found to be similar for all the polytypes, independently of the structure of the polytype. The wurtzite structure has the highest energy, whereas the 4H phase is the most stable. The charge asymmetry of a Si–C bond, on the boundary separating the zb from the wurtzite phase, together with the closeness of the total energies between the cubic and hexagonal polytypes (within 4.3 meV/atom), should be related to the polytypism of SiC. In the hexagonal polytypes, the *M* conduction band energy increases, while that of the *K* point decreases as the degree of hexagonal nature becomes more prominent. Thus,

 ©2005 The American Physical Society

the conduction band minimum state located at the X point for cubic SiC changes to the M point and then to the K point for the 2H structure.

The *ab initio* pseudopotential method has been used in calculations of ground state properties of cubic and hexagonal SiC polytypes.[15] Internal relaxations of the atomic positions result in small changes in the calculated ground state properties. Overall agreement of the theoretical values with the experimental data is reasonable whether or not atomic relaxations are included. The main effects of the relaxations are on the volume per Si–C pair and the ordering of the polytypes. Experimentally a slight decrease of the unit cell volume with hexagonality is found. Theoretically, this is only observed by inclusion of atomic relaxations. Inclusion of atomic relaxations changes the energetic ordering of the polytypes and, hence, the conclusions with respect to the polytype stability. Without atomic relaxations these calculations predict the cubic structure to be stable with respect to the wurtzite one by about 8 meV/atom. The zb structure seems to be also lower in energy than the other hexagonal polytypes 6H and 4H. However, their energy differences are smaller than 1 meV and, therefore, approach the accuracy of the calculations. Taking into account the relaxations of the cell geometries, the principal ordering of the polytypes is changed. However, the difference in the cohesive energies of the stable 4H polytype and the most unfavorable wurtzite structure approaches 3 meV/atom.

The atomic structures of the hexagonal 6H and 4H polytypes of SiC have been determined by a combination of high precision x-ray diffraction measurements and *ab initio* pseudopotential calculations.[16] The lattice parameters c and a are determined by means of the x-ray diffraction bond method using Cu $K_{\alpha 1}$ radiation. The measured fluctuations are smaller than 5×10^{-6} with respect to the average value of the parameter. The calculated lattice constants are smaller than the experimental values as is usually the case in the local density approximation (LDA). Nevertheless, the tendency for a better agreement after inclusion of the internal degrees of freedom clearly shows the importance of the atomic relaxations. Both in theory and experiment, the lattice parameter a decreases with increasing hexagonality. On the other hand c/n, n being the number of bilayers per unit cell, increases with rising hexagonality. The ratio $c/(na)$ deviates from its ideal value in 3C SiC $c/(na)=\sqrt{2/3}\simeq 0.816$ with increasing hexagonality, indicating a stronger distortion of the bonding tetrahedra. For $c/(na)$, the agreement between theory and experiment is almost perfect when including the internal relaxations in the calculation. The atomic relaxations within the unit cell are derived by means of two different kinds of pseudopotentials for 6H and 4H SiC. Structure factors, bilayer thickness fluctuations and bond length fluctuations have been compared with the experimental findings. They conclude excellent predictions from the first-principles calculations. This holds especially for the significant displacements in the hexagonal bilayers, which give important contributions to the elongation of the bonding tetrahedron parallel to the c axis. The full potential linear muffin-tin orbital (FP-LMTO) method has been used to calculate equilibrium, phonon, and elastic properties of 3C SiC.[17] Their result for the equilibrium lattice constant is 1% smaller than the measured value, as is usually the case in LDA, whereas the bulk modulus is in excellent agreement with experiment. The calculated elastic constants are in good agreement with the experimental values derived from the sound velocities of Feldman *et al.*[18]

The FP-LMTO method has also been used to carefully compare the energetics of different polytypes.[19] Using a well tested density functional and taking care to converge with respect to all relevant calculation parameters, Limpijumnong *et al.*[19] found that the 4H, 6H, and 15R structures were nearly degenerate. The 15R structure was lowest in energy and 4H was lower in energy than 6H, but all were essentially within the estimated accuracy. The 3C structure was significantly higher in energy (about 1 meV/atom), and 2H almost 3 meV/atom higher than 3C. The overall ordering is the same (for the structures in common, namely, 2H, 3C, 4H, and 6H) as that of older work in Refs. 14 and 20, although the energy differences do not agree. The results of Ref. 19 are in better agreement with the energy differences from the DFT calculations of Cheng *et al.*,[21] although the ordering of the polytypes is different. More recent results using DFT with pseudopotentials and a plane-wave basis[22] also show good agreement with the FP-LMTO calculations in Ref. 19.

We now discuss previous tight-binding (TB) calculations for SiC. A semi-empirical TB Hamiltonian has been used in an electronic structure calculation of cubic SiC.[23] A set of semi-empirical expressions for the two-center integrals is constructed for SiC, with an explicit dependence on the atomic characteristics. The merits of these semi-empirical expressions are demonstrated by the reproduction of the electronic energy bands of cubic SiC and by the application to defect problems. A claim of a self-consistent TB method has been made in calculations of binding energy, bulk modulus, and effective charge of Si and SiC.[24] This calculation incorrectly predicts the wurtzite structure as the stable structure. A second-neighbor TB scheme has been employed in electronic structure calculations of cubic SiC as well as in the numerical evaluation of the bound electronic states of isolated and complex defects in zb SiC.[25] This scheme predicts reasonably well the electronic energy bands of cubic SiC. Furthermore, comparison of the important optical gaps with experimental and theoretical data shows reasonably good agreement. The electronic and optical properties of 3C SiC have also been studied by a combination of first-principles and TB electronic structure calculations.[26] For the evaluation of the electronic properties, a pseudopotential DFT method is used, with appropriate corrections to the eigenvalues of conduction states to obtain the correct band gap. The calculated band-structure energies at points of high symmetry are in excellent agreement with experimental data. The second computational approach is the empirical TB model with a three-center orthogonal *sp* basis Hamiltonian fitted to reproduce the band structure calculated by the LDA method. This TB parametrization allowed this group to calculate the dielectric function and reflectivity. Further work[27] of this group using TB focused on free-floating and epitaxially strained $Si_{1-y}C_y$ alloys.

The above TB scheme fits only the band structure and has no total energy capability, in contrast to the work we present here. We use the NRL-TB method,[28] a nonorthogonal tight-

binding method in the two-center representation that uses environmentally dependent parameters that fit both the band structure and total energy. This method produces good structural energy differences, elastic constants, phonon frequencies, vacancy formation energies, and surface energies for a large variety of materials.[28] Hamiltonians using the NRL-TB method have been developed for C, Si, and Ge,[29–31] and applied to systems such as amorphous solids and grain boundaries that require large unit cells that are difficult to simulate directly using first-principles methods.

The remainder of the article is organized as follows. In Sec. II we describe the functional form of our TB parametrization and the fitting data set. In Sec. III we discuss applications of the TB model to a range of properties such as the ground state electronic structure of the various polytypes of SiC, band structure, density of states, and elastic constants. In addition, for cubic SiC, we performed molecular dynamics (MD) simulations at various temperatures to obtain the temperature dependence of the mean-square displacement and of the pressure. In the last section, we summarize the results.

II. FUNCTIONAL FORM AND FITTING

In this paper we present electronic structure and total energy results for a TB parametrization using a *sp* basis. We also present electronic structure results for a parametrization using a *spd* basis. Since the functional forms of the parameters used in the NRL scheme have already been presented,[28] we will only give a brief summary here. The total energy of the system is written as the sum of the energies of the occupied electronic eigenstates. The onsite Hamiltonian matrix elements vary with the local density associated with each atom, allowing the NRL-TB method to use, in the fit, linear augmented plane-wave (LAPW) eigenvalues that have been shifted so that the LAPW total energy is equal to the eigenvalue sum. Therefore, all of the contributions to the total energy are accounted for in the eigenvalue sum, and the addition of a sum of pair potentials, a feature common to most TB models, is not needed.

The energies of the electronic states and the corresponding eigenvectors are the solutions of a generalized eigenvalue equation with Hamiltonian and overlap matrix elements parametrized as follows: the basis used to describe the Hamiltonian and overlap matrices is a set of one *s* and three *p* orbitals around each atom, with all interactions between atoms assumed to be in the two-center approximation.[32] A local atomic density at atom i contributed by atoms of type J is defined as

$$\rho_{iJ} = \sum_j e^{-\lambda_J^2 |\boldsymbol{R}_j - \boldsymbol{R}_i|} f(|\boldsymbol{R}_j - \boldsymbol{R}_i|), \quad (1)$$

where j enumerates atoms of type J, $\boldsymbol{R}_i$ is the position of atom i, λ_J is a fitting parameter, and $f(R)$ is a cutoff function that is used to limit the range of the parameters. The onsite matrix element on atom i of type I is given in terms of the local atomic density as

$$h_{il} = \alpha_{Il} + \sum_J \beta_{IJl}\rho_{iJ}^{2/3} + \gamma_{IJl}\rho_{iJ}^{4/3} + \chi_{IJl}\rho_{iJ}^2, \quad (2)$$

where l is the orbital type index (s or p), and α_{Il}, β_{IJl}, γ_{IJl}, and χ_{IJl} are fitting parameters. The distance dependence of the two-center hopping matrix elements is given by

$$H_{ll'\mu}(R) = (a_{ll'\mu} + b_{ll'\mu}R + c_{ll'\mu}R^2)\exp(-g_{ll'\mu}^2 R) f(R), \quad (3)$$

where l and l' are orbital type indices, μ is an index for the type of interaction between orbitals (σ, π, or δ), and the parameters $a_{ll'\mu}$, $b_{ll'\mu}$, $c_{ll'\mu}$, and $g_{ll'\mu}$ are fitting parameters. The overlap matrix elements are given by

$$S_{ll'\mu}(R) = (\delta_{ll'} + t_{ll'\mu}R + q_{ll'\mu}R^2 + r_{ll'\mu}R^3) \times \exp(-u_{ll'\mu}^2 R) f(R) \quad (4)$$

for pairs of atoms of the same type, and by

$$S_{ll'\mu}(R) = (t_{ll'\mu} + q_{ll'\mu}R + r_{ll'\mu}R^2) \times \exp(-u_{ll'\mu}^2 R) f(R) \quad (5)$$

for pairs of atoms of different types, where $t_{ll'\mu}$, $q_{ll'\mu}$, $r_{ll'\mu}$, and $u_{ll'\mu}$ are fitting parameters.

The 134 parameters used by the functional form for the *sp* basis parametrization are fit to three high-symmetry crystal structures.[33] The fitting data set includes both the total energy and band structure for the zb and wurtzite lattices for SiC and the diamond lattice for elemental Si and C. In addition, elemental C and Si configurations with a frozen-in Γ-point optical phonon were included. The data for each lattice are for a wide range of volumes around the energy minimum. The total energy and eigenvalues of each crystal were computed by the LAPW method[34,35] *ab initio* DFT calculations. For the exchange-correlation potential, we used the LDA functional of Perdew and Wang.[36] The wurtzite lattice data included the widest range of volumes, from 29.64 to 53.35 Å^3, and the zb lattice from 16.91 to 26.11 Å^3. The diamond lattice structures ranged from 31.78 to 45.39 Å^3 for elemental Si and from 8.00 to 13.83 Å^3 for elemental C. The *spd* parametrization was fitted to only two structures: 3C at a volume of 20.43 Å^3 and 2H at a volume of 40.75 Å^3.[33] Since the *spd* parametrization is intended for electronic structure calculations, we fit only to a corrected LAPW band structure, which has been adjusted to match the experimental band gap by shifting the conduction band states rigidly by 0.079 Ry.

We performed these LAPW calculations for the purpose of generating the database for the TB fit. However, we wish to point out that while there are several pseudopotential and LMTO calculations for SiC in the literature, there are no comprehensive LAPW results except for a study of Ti impurities in SiC.[37]

III. RESULTS

A. Structures

The LAPW results described in the previous section were used as a database to construct the TB Hamiltonian. The

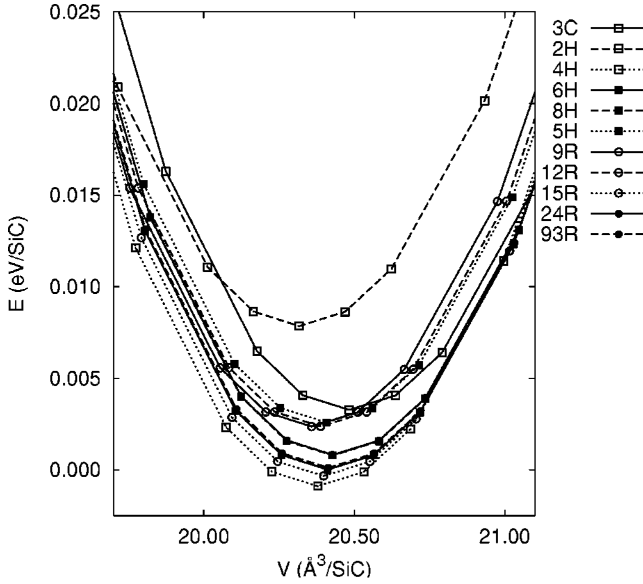

FIG. 1. Total energy vs. volume per SiC pair for a number of polytypes, computed using the TB model.

overall rms fitting error for the total energies of all the fitted structures is 2.0 mRy. The TB ground state total energies as a function of volume per SiC pair for a range of structures are shown in Fig. 1. Convergence of the relaxed energy with respect to k-point sampling is about 5 μeV per SiC formula unit, much smaller than the polytype energy differences. The minimum energies for each structure are listed in Table I, along with our LAPW calculations and recent literature DFT calculation values.[14,19,22,38] It is clear from the table that the energy differences between polytypes are quite small, and that first-principles calculations disagree on the quantitative values. Even the ordering in energy and the ground state structure are not consistent among the different DFT calculations. However, it is clear that the 4H or 6H (moderately hexagonal) structures are lowest in energy, 2H (fully hexagonal) is probably highest, and 3C (no hexagonal stacking) is in the middle. It is remarkable that the TB model can capture the correct ordering by fitting only the cubic 3C and fully hexagonal 2H phases, given that the energy varies nonmonotonically with the degree of hexagonal stacking.

This model correctly predicts the lowest energy state to be the 4H structure. The highest total energy was obtained for 2H SiC, which may be one explanation as to why this polytype, of the ones studied here, is the most difficult to grow. We have included the hypothetical rhombohedral 9R polytype because of its high degree of hexagonal nature (it is 66% hexagonal). Our TB model correctly predicts the energy of the 9R structure to be lower than wurtzite, although in contradiction with previous work, we find that it is also lower in energy than zb. This small discrepancy may be caused by a tendency of our TB model to overestimate the energy gains from alternating cubic and hexagonal stacking, also seen in the low energy of the 4H structure relative to the cubic zb.

The TB calculations predict the equilibrium lattice parameters a and c in excellent agreement with the experimental ones. The results are shown in Table II. From Table II we observe that both in theory and experiment, the lattice parameter a of the hexagonal polytypes increases with decreasing hexagonality. This trend is in agreement with recent experimental and theoretical work.[16] Lattice parameters of 3C, 2H, 4H, and 6H SiC, calculated with the pseudopotential density-functional method, have been collected in Table II. As Table II shows, our results are comparable in accuracy with the pseudopotential calculation of Ref. 14. The lattice constants, bulk moduli, and Raman mode frequencies of Si and C in the diamond structure, which are also in the fitting database, are described reasonably well.

TABLE I. Relative energies (meV/SiC) of SiC polytypes computed with the TB model, our LAPW calculations, and published plane-wave pseudopotential (PP) DFT values.

Struct.	PP	LAPW	TB
4H	−2.5,[a] −0.93,[b] −2.4,[c] −2.4[d]	−1.7	−4.2
6H	−1.8,[a] −0.63,[b] −2.1,[c] −2.2[d]		−3.2
93R			−3.2
8H			−2.5
24R			−2.5
9R	2.0[c]		−0.9
12R			−0.9
15R	−3.0[c]		−3.6
5H			−0.7
3C	0.0	0.0	0.0
2H	1.8,[a] −0.65,[b] 5.4,[c] 6.0[d]	4.6	4.6

[a]From Ref. 14.
[b]From Fig. 3 in Ref. 38.
[c]From Ref. 19.
[d]From Ref. 22.

B. Electronic structure

The TB band structure of 3C SiC along directions of high crystal symmetry is shown in Fig. 2. In comparison with the LAPW band structure, shown on the same graph, our calculation correctly predicts the valence band maximum at the Γ point (slightly displaced toward Σ) and the conduction band minimum at the X point of the Brillouin zone. While our TB fit produces nearly perfect agreement with the LAPW valence bands, there are serious discrepancies in the conduction band. This is reflected in the rms fitting error for the seven volumes that we have fitted of 20 mRy for the valence bands and 69 mRy for the conduction bands. This is expected since the conduction band has significant d character that is neglected in our sp TB basis. The TB gap is 1.33 eV, in good agreement with the LAPW gap of 1.31 eV. Both gaps are much smaller than the experimental value of 2.39 eV,[40] due to the use of the LDA in LAPW theory. The TB band structure is very similar to previous ones,[41–44] all of them have the same shape with a strong parabolic behavior around the conduction band minimum. The indirect energy gaps vary from 1.20 eV in the LMTO calculation[42] to 2.59 eV in the quasi-

TABLE II. Lattice parameters for SiC polytypes, computed with the *sp* TB model, and comparison with available experimental, pseudopotential (PP), and LAPW DFT values. The lattice parameter c is normalized by n, the number of SiC bilayers per unit cell. The structure 3C′ indicates the zinc-blende in a rhombohedral supercell, for comparison with the other structures.

	TB		Exp.[a]		PP		LAPW	
Struct.	a(Å)	c/n(Å)	a(Å)	c/n(Å)	a(Å)	c(Å)	a(Å)	c(Å)
Zinc-blende (3C)	4.3432		4.3581		4.365[b]		4.343	
					4.323[c]			
					4.358[d]			
					4.291[e]			
Zinc-blende (3C′)	3.0711	2.5070	3.0816	2.5162	3.087[b]	2.520[b]	3.071	2.507
					3.057[c]	2.496[c]		
					3.082[d]	2.516[d]		
					3.034[e]	2.477[e]		
Wurtzite (2H)	3.0568	2.5106	3.0760	2.5240	3.120[f]	2.515[f]	3.057	2.511
					3.072[d]	2.521[d]		
					3.031[e]	2.480[e]		
9R	3.0611	2.5088						
12R	3.0635	2.5084						
15R	3.0647	2.5088						
24R	3.0671	2.5076						
93R	3.0659	2.5076						
4H	3.0632	2.5078	3.0805	2.5212	3.069[d]	2.526[d]	3.063	2.507
					3.032[e]	2.482[e]		
5H	3.0650	2.5083						
6H	3.0658	2.5076	3.0807	2.5196	3.077[d]	2.518[d]		
					3.033[e]	2.480[e]		
8H	3.0671	2.5076						

[a]Reference 39, except 4H from Ref. 16.
[b]Reference 11.
[c]Reference 12.
[d]Reference 14.
[e]Reference 15.
[f]Reference 13.

particle one.[43] In the pseudopotential calculations of Käckell *et al.*[45] and Park *et al.*[14] the 3C SiC bands are presented in a hexagonal cell, with indirect gaps 1.27 and 1.24 eV, respectively.

The comparison between the TB density of states (DOS) and the LAPW DOS is demonstrated in Fig. 3. The TB model correctly describes the valence band: positions and heights of peaks are in very good agreement with the corresponding peaks in the LAPW valence band. However, in the conduction band, there are differences due to unoccupied orbitals with strong *d* character. The partial DOS functions show that the strongest contribution to the total DOS comes from Si *s* and C *p* bands.

The comparison between the TB DOS and the LAPW DOS of the hexagonal polytype of SiC(2H) is shown in Fig. 4, and the corresponding band structures are shown in Fig. 2. In the TB valence band the positions and the heights of the peaks are in excellent agreement with the corresponding peaks in the LAPW valence band. However, in the conduction band, peak heights are only in fair agreement. In contrast to previous calculations,[14,43–46] the conduction band minimum is predicted at the M point of the Brillouin zone and this accounts for the discrepancies near the Fermi level. The TB gap is 3.07 eV, whereas the LAPW one is 2.11 eV. Compared with the experimental value of 3.33 eV,[47] the underestimation of the LAPW band gap is known to result from the use of the LDA in our calculations. The agreement of the TB gap with experiment is fortuitous.

Most of the results in this paper depend on the occupied states of SiC. However, there are situations such as in studies of optical properties where there is a need to have an accurate representation of the conduction band as well as the correct value of the energy gap. We have addressed this issue by adjusting the LAPW gap to the experimental value and fitting a TB Hamiltonian with a *spd* basis. The rms fitting errors are 12 mRy for the eight bands that we have fitted for the 3C structure, and 12 mRy for the 16 bands we have fitted for the 2H structure. The resulting energy bands for the 3C and 2H structures at the fitted volumes are shown in Fig. 5. One can see that we now have an almost perfect fit of both the valence and conduction bands.

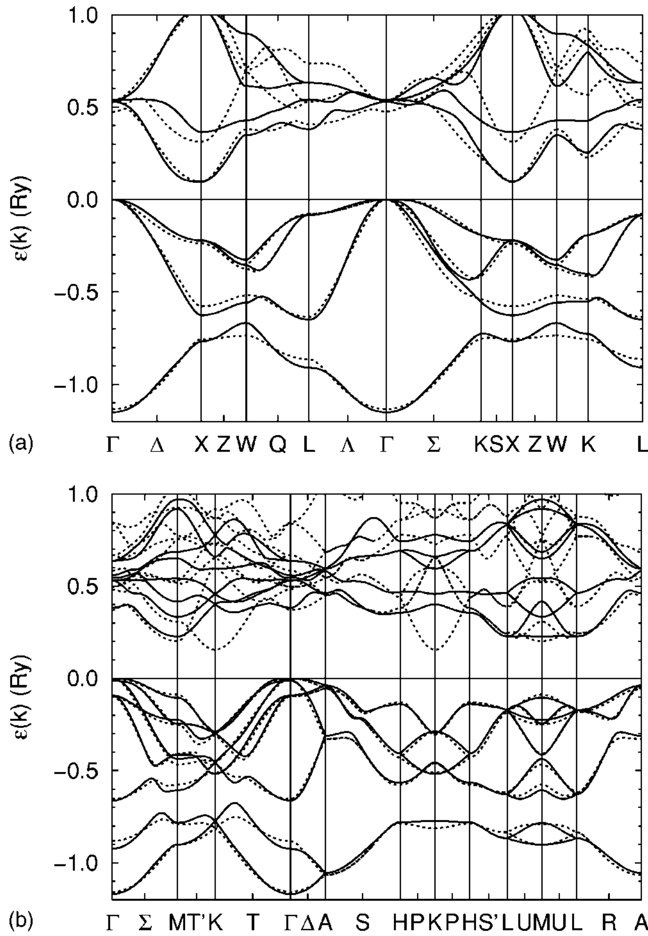

FIG. 2. Band structure along high-symmetry directions in the Brillouin zone for 3C SiC (top) and 2H SiC (bottom). Solid lines are TB *sp* results, dashed lines are LAPW-LDA results. All energies are referenced to the valence band maximum.

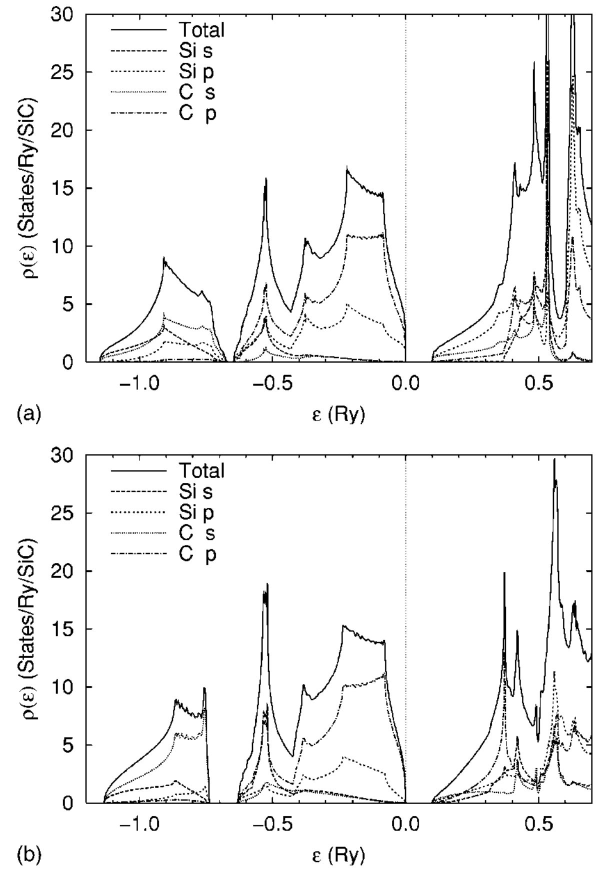

FIG. 3. Total and partial TB densities of states for 3C SiC. The top panel shows TB *sp* results, and the bottom panel shows LAPW results.

C. Elastic constants and phonons

The elastic constants c_{ij} contain some of the most important information that can be obtained from ground state total energy calculations. A given crystal structure cannot exist in a stable or metastable phase unless its elastic constants obey certain relationships. The c_{ij} also determine the response of the crystal to external forces and thus play an important part in determining the strength of a material. The procedure for calculating elastic constants from first-principles calculations is described by Mehl *et al.*[49] The same procedure is used in our TB calculations. Briefly, one imposes an external strain on the crystal and calculates the energy as a function of strain. Our method correctly gives the experimental value for the bulk modulus and elastic constants for 3C SiC, as shown in Table III. The agreement between our calculated values and the experimental data for 3C SiC is quite good given that these are not fitted quantities. As Table III shows, our results are comparable in accuracy to the LDA calculations of Ref. 17. For 4H SiC the agreement with experiment is excellent as well. We also present as a prediction the elastic constants for the 2H structure.

The phonon spectrum for the 3C structure along the high-symmetry Γ-L direction was computed using the frozen phonon method. The results, in comparison with experiment,[18] are plotted in Fig. 6. Results for the acoustic modes are in very good agreement with experiment. Zone-edge frequencies for the optical modes are also in good agreement with experiment, although about 150 cm^{-1} low. The splitting between the transverse and longitudinal optical modes is not captured by the TB model. This is expected, given that the splitting is caused by charge redistribution effects that can only be described by explicit Coulomb terms in the Hamiltonian. The transverse optical mode at the Γ point is in very good agreement with experiment[18] and with previous first-principles phonon frequency calculation for SiC.[17,50,51]

D. Stacking faults

The interesting energetic properties of the polytypes of SiC are directly related to the stacking fault (SF) energetics. A SF in an otherwise cubic structure is equivalent to a locally hexagonal structure, and vice versa. Therefore, the overall energy ordering of the polytypes, where some hexagonality is favored over perfect cubic stacking (e.g., 4H is lower in energy than 3C), can be explained if the SF energy in the cubic structure is negative, favoring the spontaneous formation of some hexagonal stacking. The status of 4H as the lowest energy polytype should be associated with positive energy SFs. We used our TB model, which was fitted to only

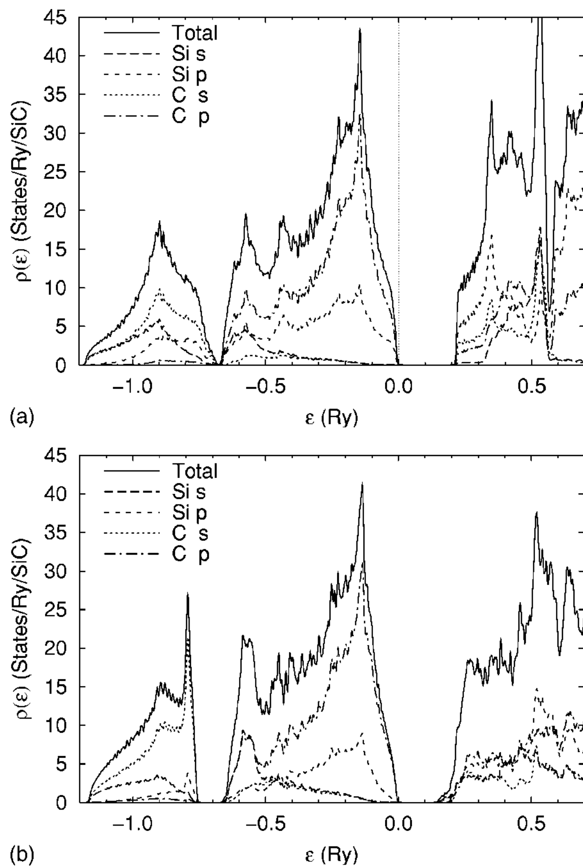

FIG. 4. Total and partial DOS for 2H SiC. Top panel shows TB *sp* results, and bottom panel shows LAPW results.

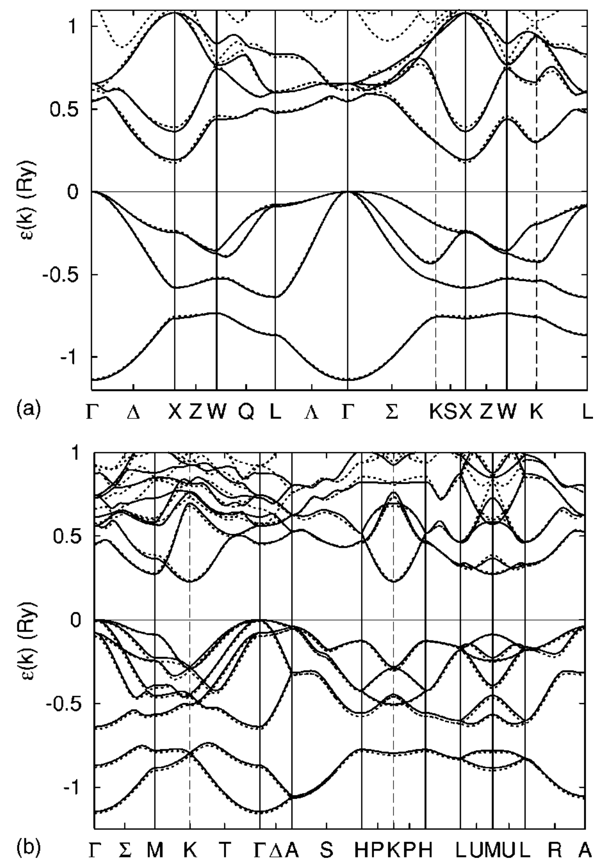

FIG. 5. Band structure along high-symmetry directions in the Brillouin zone for 3C SiC (top) and 2H SiC (bottom). Solid lines are TB *spd* results, dashed lines are shifted LAPW LDA results. All energies are referenced to the valence band maximum.

the perfect 3C and 2H structures, to calculate SF energies in the 3C and 4H structures. Unit cells composed of 12 bilayers with and without a SF are relaxed with respect to atomic positions and lattice constant normal to the SF plane using the conjugate gradient method.[52] The results are shown in Table IV, together with DFT calculation results. There is significant variation in the calculated magnitude of the intrinsic SF formation energy in 3C SiC, as shown in Table II of Ref. 53. Our TB calculations show a small negative formation energy, in agreement with direct calculations using DFT methods.[53,54] The 4H polytype shows positive formation energy for both geometrically inequivalent SFs, in agreement with direct DFT calculations, although the magnitude of the energy is somewhat large. Even the ordering between the two inequivalent SFs, which involves very small energy differences, is in agreement with DFT calculations. Overall, the agreement between our TB calculations and DFT results is quite good, especially considering the fact that there was no information about isolated stacking faults in the fitting database.

E. Vacancies

The properties of materials with significant covalent bonding such as SiC are often dominated by point defects, which allow for lattice rearrangement during diffusion, and can be electronically active. We simulated vacancies in 3C SiC using a periodic supercell approach. We computed the energies of a 216-atom cubic supercell, and the same supercell with one C or one Si atom removed. Each configuration was relaxed with a conjugate-gradient energy minimization algorithm.[52] To use these energies to compute the formation energy of a vacancy E_f we assume that the SiC solid is in

TABLE III. Elastic constants and bulk moduli in GPa for 3C, 4H, and 2H SiC polytypes, computed with the *sp* TB model, FP-LMTO, and experiment.

	3C			4H		2H
	TB	FP-LMTO[a]	Exp.[b]	TB	Exp.[c]	TB
B	220	223	225	221	221	221
c_{11}	386	420	390	476	507	481
c_{12}	137	126	142	123	108	127
c_{13}				72	52	58
c_{33}				521	547	522
c_{44}	220	287	256	150	159	143
c_{66}				177		177

[a]Reference 17.
[b]The experimental data are derived by Lambrecht *et al.* (Ref. 17), from the sound velocities of Feldman *et al.* (Ref. 18).
[c]Reference 48.

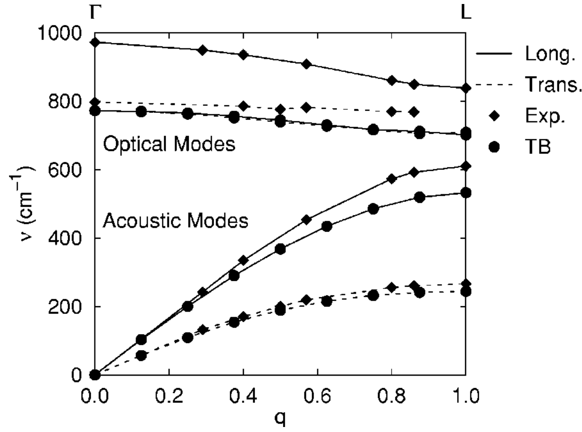

FIG. 6. Phonon dispersion curves for the 3C structure along the Γ-*L* direction. Solid lines indicate longitudinal modes and dashed lines indicate transverse modes. Circles indicate TB results and diamonds indicate experimental results from Ref. 18.

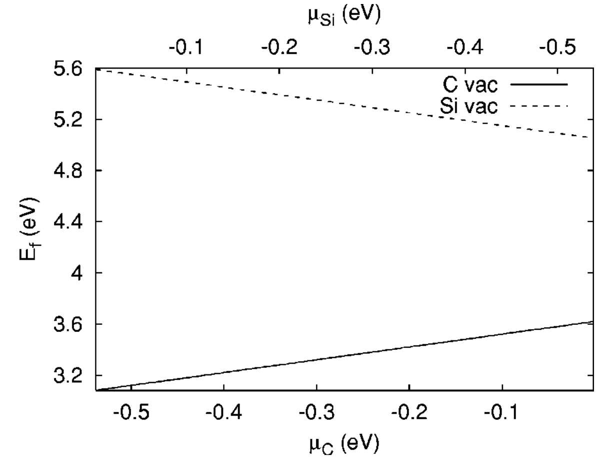

FIG. 7. Relaxed formation energy (eV) for C and Si vacancies in 3C SiC, as a function of C chemical potential μ_C(eV) (or equivalently, the Si chemical potential μ_{Si}).

equilibrium with reservoirs of C and Si at chemical potentials μ_C and μ_{Si}, respectively. The vacancy formation energy is defined as

$$E_f = E^v - N_C\mu_C - N_{Si}\mu_{Si}, \tag{6}$$

where E^v is the energy of the configuration with a vacancy, and N_C and N_{Si} are the numbers of C and Si atoms, respectively, in the vacancy configuration. Because the bulk SiC solid is in equilibrium with respect to the two elemental reservoirs, the two elemental chemical potentials are related through

$$\mu^0_{SiC} = \mu_C + \mu_{Si}, \tag{7}$$

where μ^0_{SiC} is the energy per formula unit of bulk SiC. The elemental chemical potentials are constrained because each reservoir must be stable with respect to the pure bulk solid, giving

$$\mu_C \leqslant \mu^0_C, \tag{8}$$

$$\mu_{Si} \leqslant \mu^0_{Si}, \tag{9}$$

where μ^0_C and μ^0_{Si} are the energies per atom of bulk diamond-structure C and Si. Combining Eqs. (7)–(9) yields the constraint

$$\mu^0_{SiC} - \mu^0_{Si} \leqslant \mu_C \leqslant \mu^0_C, \tag{10}$$

and an equivalent expression for μ_{Si}. The formation energy can be computed in terms of either μ_C or μ_{Si} (since the two are related), over a range of physically meaningful values limited by the stability of the C and Si reservoirs with respect to the two pure bulk solids.

The results in Fig. 7 indicate that C vacancies are lower in energy than Si vacancies throughout the composition range. Formation energies vary from 3.1 to 3.6 eV for the C vacancy and 5.1 to 5.6 eV for the Si vacancy. These values are in reasonable agreement with the DFT calculations of Furthmüller *et al.*, who found C vacancy energies of about 4 to 4.5 eV and Si vacancy energies of 8.5 to 9 eV.[55] Two other groups[56,57] get similar results using DFT calculations. Both quote only vacancy formation energies at $\mu_C = \mu_{Si}$, with values of 5.48 and 5.9 eV for E_f^C and 6.8 and 6.64 eV for E_f^{Si}, in reasonable agreement with our calculations of $E_f^C = 3.4$ eV and $E_f^{Si} = 5.3$ eV.

The geometries of the relaxed vacancies show the distinct asymmetry between the two atomic species. The Si atoms around the C vacancy relax outward in a breathing mode, moving by about 0.02 Å. Apparently the potential energy gain from bonding through the dangling bonds, the mechanism that leads to the Jahn-Teller distortion in Si, is not strong large to overcome the stiffness of the Si–C backbonds. The C atoms around the Si vacancy relax much more, moving outward and breaking the symmetry by forming a triangular pyramid with 3.55 Å bonds within the base and 3.78 Å bonds to the vertex. This allows three of the C atoms to have three nearly planar bonds (bond angles of 118°), and the fourth to be between tetrahedral and planar (bond angles of 113°). Presumably this relaxation is driven by the stability of the C atoms in planar sp^2 hybridization. A full treatment of the vacancy would require spin polarization and the examination of different charge states (beyond the neutral vacancy simulated here), but these extend beyond the scope of this work.

TABLE IV. Relaxed stacking fault energies (mJ/m^2) computed using the TB model, compared with published DFT calculation values.

SF	TB	DFT
3C (intrinsic)	−4.44	−1.71, [a] −3.4[b]
4H(31)	25.4	17.7[a]
4H(13)	25.6	18.1[a]

[a]From Ref. 52.
[b]From Ref. 53.

F. Molecular dynamics simulations

An important advantage of our TB approach is that we can perform MD simulations reasonably quickly for rela-

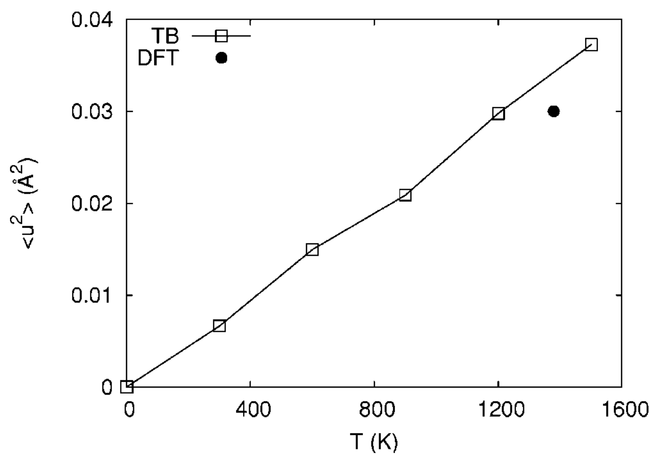

FIG. 8. Mean-square displacement as a function of temperature for 3C SiC, derived from MD simulations using our TB model. Result of DFT is from the quasiharmonic approximation calculation of Ref. 58.

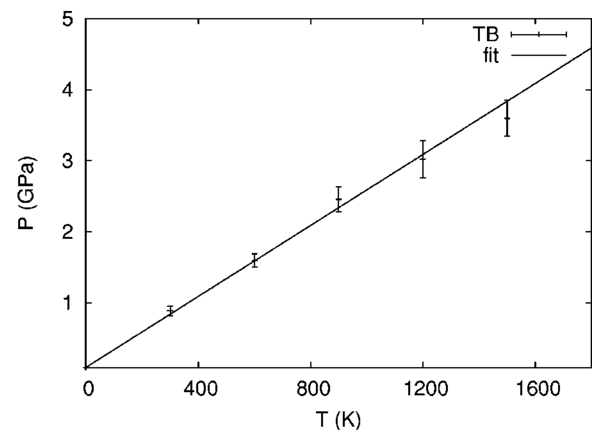

FIG. 9. Pressure as a function of temperature for 3C SiC at the $T=0$ K equilibrium lattice constant, derived from MD simulations using our TB model.

tively large number of atoms and therefore obtain temperature-dependent quantities. The standard LDA MD calculations can only be done for very small systems and therefore they are not reliable. We performed MD simulations for the cubic polytype of SiC. In our simulations, the system consists of an fcc supercell of 512 atoms. The equations of motion were integrated using a time step of 2 fs for 2000 steps, 1000 time steps for equilibration, and 1000 time steps where data were gathered. We performed MD simulations for several temperatures at the TB equilibrium lattice constant, $a=4.343$ Å, to compute the mean-square displacements of the atoms and the thermal expansion coefficient.

In Fig. 8, we show mean-square displacement as a function of temperature as derived from the simulations. The results are in good agreement with the plane-wave pseudopotential DFT calculations of Karch *et al.*,[58] who used a quasiharmonic approximation to estimate the mean-square displacements since MD was not practical. The agreement is expected given the intermediate range of temperatures compared, significantly above the Debye temperature but significantly below the melting point (3100 K).[59] The results of the thermal expansion coefficient measurements are plotted in Fig. 9 in the form of the pressure as a function of temperature at the $T=0$ K equilibrium lattice constant. From the fit, we can extract $\partial P/\partial T$, and from that the linear thermal expansion coefficient $\alpha=3.8\times10^{-6}$ K^{-1}. A quasiharmonic approximation derived by minimizing the volume derivative of the free energy (computed in terms of the phonon frequencies as a function of volume[60]) gives a very similar value for α of 3.9×10^{-6} K^{-1}. Both results are in reasonable agreement with the quasiharmonic approximation DFT high-temperature value of about 5×10^{-6} K^{-1}.[58]

IV. CONCLUSIONS

We have applied the NRL-TB method to generate a *sp* basis TB model for SiC that was fitted to LAPW results of high-symmetry crystal structures of SiC, Si, and C and the Raman phonon mode of C and Si, and a *spd* basis TB model that was optimized for the electronic properties of the cubic zb and hexagonal wurtzite structures. We found that the resulting *sp* Hamiltonian is transferable to a wide range of polytypes, capturing the nonmonotonic energy variation with respect to hexagonal character despite being fitted only to a fully cubic and a fully hexagonal structure. This model also correctly describes valence band electronic properties (band structure and density of states). The *spd* model reproduces both the valence and conduction bands of the cubic and wurtzite structures, at the expense of a lack of transferability to other properties. The *sp* model reproduces experimental measurements for elastic constants, phonon frequencies, stacking fault energies, and vacancy formation energies. In addition, we performed molecular dynamics simulations at various temperatures to compute the mean-square displacement and thermal expansion coefficient, both in good agreement with experiment and previous simulations. It is stressed that the NRL-TB method, because of its computational efficiency, can be very useful in the study of phenomena which require the use of large unit cells. In addition to the bulk energetic properties of polytypes we presented here, this method can be directly applied to surface properties that can dominate polytype selectivity during growth. It is hoped that with the present set of parameters, the method can be used to study other complex structural and electronic effects that are experimentally observed in SiC.

ACKNOWLEDGMENTS

This work was supported by the U.S. Office of Naval Research, the Naval Research Laboratory, and the Common High Performance Computing Software Support Initiative (CHSSI) of the United States Department of Defense High Performance Computing Modernization Program Office (HPCMPO). The work of H.J.G. was supported by the National Research Council Associateship Program.

*Current address: Department of Physics, California State University Northridge, Northridge, CA 91330-8268.

[1] N. W. Jepps and T. F. Page, in *Crystal Growth and Characterization of Polytype Structures*, Progress in Crystal Growth and Characterization, Vol. 7, edited by P. Krishna (Pergamon, Oxford, 1983).
[2] K. Shenai, R. S. Scott, and B. J. Baliga, IEEE Trans. Electron Devices **36**, 1811 (1989).
[3] J. H. Edgar, J. Mater. Res. **7**, 235 (1992).
[4] G. Pensl and Th. Troffer, Solid State Phenom. **47–48**, 115 (1996).
[5] J. B. Casady and R. W. Johnson, Solid-State Electron. **39**, 1409 (1996).
[6] See, e.g., *Silicon Carbide and Related Materials 2001* in Materials Science Forum Vol. 389–393, edited by S. Yoshida, S. Nishino, H. Harima, and T. Kimoto (Trans Tech., Zurich, Switzerland, 2002), and references therein.
[7] J. von Boehm and P. Bak, Phys. Rev. Lett. **42**, 122 (1979).
[8] C. Cheng, R. J. Needs, and V. Heine, J. Phys. C **21**, 1049 (1988).
[9] V. Heine, C. Cheng, and R. J. Needs, Mater. Sci. Eng., B **11**, 55 (1992).
[10] V. Heine, C. Cheng, G. F. Engel, and R. J. Needs, in *Wide Band Gap Semiconductors*, MRS Symposia Proceedings No. 242, edited by T. D. Moustakas, J. I. Pankove, and Y. Hamakawa (Materials Research Society, Pittsburgh, PA, 1992), p. 507.
[11] P. J. H. Denteneer and W. van Haeringen, Phys. Rev. B **33**, 2831 (1986).
[12] N. Churcher, K. Kunc, and V. Heine, J. Chem. Phys. **19**, 4413 (1986).
[13] P. J. H. Denteneer and W. van Haeringen, Solid State Commun. **65**, 115 (1988).
[14] C. H. Park, B.-H. Cheong, K.-H. Lee, and K. J. Chang, Phys. Rev. B **49**, 4485 (1994).
[15] P. Käckell, B. Wenzien, and F. Bechstedt, Phys. Rev. B **50**, 17 037 (1994).
[16] A. Bauer, J. Kräusslich, L. Dressler, P. Kuschnerus, J. Wolf, K. Goetz, P. Käckell, J. Furthmüller, and F. Bechstedt, Phys. Rev. B **57**, 2647 (1998).
[17] W. R. L. Lambrecht, B. Segall, M. Methfessel, and M. van Schilfgaarde, Phys. Rev. B **44**, 3685 (1991).
[18] D. W. Feldman, J. H. Parker, Jr., W. J. Choyke, and L. Patrick, Phys. Rev. **170**, 698 (1968); Phys. Rev. **173**, 787 (1968).
[19] S. Limpijumnong and W. R. L. Lambrecht, Phys. Rev. B **57**, 12017 (1998).
[20] P. Käckell, B. Wenzien, and F. Bechstedt, Phys. Rev. B **50**, 17 037 (1994).
[21] C. Cheng, V. Heine, and R. J. Needs, J. Phys.: Condens. Matter **2**, 5115 (1990).
[22] M. J. Rutter and V. Heine, J. Phys.: Condens. Matter **9**, 8213 (1997).
[23] Y. Li and P. J. Lin-Chung, Phys. Rev. B **36**, 1130 (1987).
[24] M. Kohyama, S. Kose, M. Kinoshita, and R. Yamamoto, J. Phys.: Condens. Matter **2**, 7791 (1990).
[25] D. N. Talwar and Z. C. Feng, Phys. Rev. B **44**, 3191 (1991).
[26] G. Theodorou, G. Tsegas, and E. Kaxiras, J. Appl. Phys. **85**, 2179 (1999).
[27] G. Theodorou, G. Tsegas, P. C. Kelires, and E. Kaxiras, Phys. Rev. B **60**, 11 494 (1999).
[28] R. E. Cohen, M. J. Mehl, and D. A. Papaconstantopoulos, Phys. Rev. B **50**, 14 694 (1994); M. J. Mehl and D. A. Papaconstantopoulos, *ibid.* **54**, 4519 (1996); M. J. Mehl and D. A. Papaconstantopoulos, in *Topics in Computational Materials Science*, edited by C. Y. Fong (World Scientific, Singapore, 1998); D. A. Papaconstantopoulos and M. J. Mehl, J. Phys.: Condens. Matter **15**, R413 (2003).
[29] D. A. Papaconstantopoulos, M. J. Mehl, S. C. Erwin, and M. R. Pederson, in *Tight-Binding Approach to Computational Materials Science*, MRS Symposia Proceedings No. 491, edited by P. Turchi, A. Gonis, and L. Colombo (Material Research Society, Pittsburgh, PA, 1998), p. 221.
[30] N. Bernstein, M. J. Mehl, D. A. Papaconstantopoulos, N. I. Papanicolaou, M. Z. Bazant, and E. Kaxiras, Phys. Rev. B **62**, 4477 (2000).
[31] N. Bernstein, M. J. Mehl, and D. A. Papaconstantopoulos, Phys. Rev. B **66**, 075212 (2002).
[32] W. A. Harrison, *Electronic Structure and the Properties of Solids* (Dover, New York, 1989).
[33] The NRL-TB parameters used in this study for silicon carbide are available at http://cst-www.nrl.navy.mil/bind/csi.html
[34] O. K. Andersen, Phys. Rev. B **12**, 3060 (1975).
[35] S. H. Wei and H. Krakauer, Phys. Rev. Lett. **55**, 1200 (1985).
[36] J. P. Perdew and Y. Wang, Phys. Rev. B **45**, 13 244 (1992).
[37] K. O. Barbosa, W. V. M. Machado, and L. V. C. Assali, Physica B **308–310**, 726 (2001).
[38] F. Bechstedt, K. Käckell, A. Zywietz, K. Karch, B. Adolph, K. Tenelsen, and J. Hurthmüller, Phys. Status Solidi B **202**, 35 (1997).
[39] P. Villars and L. D. Calvert, *Pearson's Handbook of Crystallographic Data for Intermetallic Phases*, 2nd ed. (ASM International, Cleveland, 1991).
[40] W. J. Choyke, D. R. Hamilton, and L. Patrick, Phys. Rev. **133**, A1163 (1964).
[41] M. Rohlfing, P. Krüger, and J. Pollmann, Phys. Rev. B **48**, 17 791 (1993).
[42] M. Willatzen, M. Cardona, and N. E. Christensen, Phys. Rev. B **51**, 13 150 (1995).
[43] B. Wenzien, G. Cappellini, and F. Bechstedt, Phys. Rev. B **51**, 14 701 (1995); B. Wenzien, P. Käckell, F. Bechstedt, and G. Cappellini, *ibid.* **52**, 10 897 (1995).
[44] C. Persson and U. Lindefelt, Phys. Rev. B **54**, 10 257 (1996); J. Appl. Phys. **82**, 5496 (1997).
[45] P. Käckell, B. Wenzien, and F. Bechstedt, Phys. Rev. B **50**, 10 761 (1994).
[46] V. I. Gavrilenko, A. V. Postnikov, N. I. Klyui, and V. G. Litovchenko, Phys. Status Solidi B **162**, 477 (1990).
[47] L. Patrick, D. R. Hamilton, and W. J. Choyke, Phys. Rev. **143**, 526 (1966).
[48] K. Kamitani, M. Grimsditch, J. C. Nipko, C.-K. Loong, M. Okada, and I. Kimura, J. Appl. Phys. **82**, 3152 (1997).
[49] M. J. Mehl, Phys. Rev. B **47**, 2493 (1993); M. J. Mehl, B. A. Klein, and D. A. Papaconstantopoulos, in *Intermetallic Compounds: Principles and Applications*, edited by J. H. Westbrook and R. L. Fleischer (Wiley, London, 1994), Vol. 1, Chap. 9.
[50] K. Karch, P. Pavone, W. Windl, O. Schütt, and D. Strauch, Phys. Rev. B **50**, 17 054 (1994).
[51] C. Z. Wang, R. Yu, and H. Krakauer, Phys. Rev. B **53**, 5430 (1996).
[52] W. H. Press, B. P. Flannery, S. A. Teukolsky, and W. T. Vetterling, *Numerical Recipes in C*, 2nd ed. (Cambridge University Press, Cambridge, 1992), p. 420.

[53] H. Iwata, U. Lindefelt, S. Öberg, and P. R. Briddon, J. Phys.: Condens. Matter **14**, 12733 (2002).
[54] P. Käckell, J. Furthmüller, and F. Bechstedt, Phys. Rev. B **58**, 1326 (1998).
[55] J. Furthmüller, A. Zywietz, and F. Bechstedt, Mater. Sci. Eng., B **61–62**, 244 (1999).
[56] C. Wang, J. Bernholc, and R. F. Davis, Phys. Rev. B **38**, 12 752 (1988).
[57] F. Gao, E. J. Bylaska, W. J. Weber, and L. R. Corrales, Nucl. Instrum. Methods Phys. Res. B **180**, 286 (2001).
[58] K. Karch, P. Pavone, W. Windl, D. Strauch, and F. Bechstedt, Int. J. Quantum Chem. **56**, 801 (1995).
[59] *CRC Handbook of Chemistry and Physics*, 3rd electronic ed., edited by D. R. Lide (CRC Press, Boca Raton, FL, 2000).
[60] N. W. Ashcroft and N. D. Mermin, *Solids State Physics* (Saunders College Publishing, Fort Worth, 1976), p. 490.